Simulation of Diurnal Variation in a Stratocumulus-capped Marine Boundary Layer during FIRE

PETER G. DUYNKERKE

Utrecht University, Institute for Marine and Atmospheric Research Utrecht, Utrecht, the Netherlands

PHILLIP HIGNETT

Meteorological Research Flight, Farnborough, Hampshire, United Kingdom

(Manuscript received 11 December 1992, in final form 1 June 1993)

ABSTRACT

A model simulation is presented of the diurnal cycle of a marine stratocumulus-capped boundary layer. The model results are compared with observations obtained during the 1987 First ISCCP (International Satellite Cloud Climatology Project) Regional Experiment marine stratocumulus project, made from San Nicolas Island, off the coast of California. Both the simulation and the observations show a marked diurnal variation in cloud properties, as a result of the decoupling of the boundary layer into a separate cloud and a subcloud layer. In the model simulation the decoupling is caused by the absorption of the solar radiation in the cloud layer.

1. Introduction

The important physical mechanisms that control the structure and type of stratocumulus are cloud-top entrainment instability (CTEI), diurnal decoupling and subsequent clearing due to solar absorption and mixing with dry air from above the inversion, drizzle, mesoscale circulations, and subsidence.

We will focus on the effect of solar absorption on the decoupling and the effect of subsidence. Solar heating in the cloud can cause decoupling of the cloud layer from the subcloud layer. In a given situation, the tendency of the cloud layer and subcloud layer to become decoupled is promoted by significant shortwave absorption by the cloud and by small surface buoyancy fluxes. This implies a seasonal dependence, decoupling being more likely in summer than in winter at midlatitudes (Duynkerke 1989). However, the sun may remain sufficiently high in the subtropics for decoupling to remain possible at any time of the year.

During FIRE [First ISCCP (International Satellite Cloud Climatology Project) Regional Experiment] this decoupling was manifest as a weak stable layer that was observed below the main stratocumulus deck (Betts 1989; Hignett 1991). Below this stable layer were very often cumuli that penetrated through this stable layer into the stratocumulus above. This can under certain conditions lead to the breakup of the solid stratocumulus deck. Turbulence closure models (Bougeault 1985; Duynkerke and Driedonks 1987; Duynkerke 1989) predict this decoupling and simulate the thinning of the cloud layer during the afternoon. Here, we will assess in more detail the dynamical role.

If the subsidence is sufficiently strong, the inversion height can be lower than the mixed-layer lifting condensation level (LCL). In FIRE I the large-scale vertical velocity field was not measured systematically. This makes direct comparison of model results and observations difficult.

The purpose of this paper is to study the diurnal cycle of a marine stratocumulus layer and to make a comparison between the results of a model simulation (Duynkerke and Driedonks 1987, 1988; Duynkerke 1988) and detailed observations. We will use the observations made during the 1987 FIRE marine stratocumulus experiment. More specifically, we will use cloud-base height, inversion height, liquid water path, soundings of temperature and humidity, etc. Moreover, we will employ turbulence measurements made using instruments attached to the cable of a tethered balloon (Hignett 1991). Some of the turbulence data was already discussed by Hignett (1991); part of the data is presented here for the first time.

2. Model description

The model has been described in detail in Duynkerke and Driedonks (1987, 1988) and Duynkerke (1988). The one-dimensional model uses ensemble-averaged equations for the horizontal velocities u and v, the wet equivalent potential temperature θ_q (see Pointin 1984),

Corresponding author address: Dr. Peter G. Duynkerke, Utrecht University, Institute for Marine and Atmospheric Research, Utrecht, P.O. Box 80.005, 3508 TA Utrecht, the Netherlands.

and the total water content q_w. The vertical velocity must be prescribed. The turbulent fluxes are modeled with the gradient approach, in which the exchange coefficient is calculated from the turbulent kinetic energy E and the viscous dissipation ϵ, the so-called E–ϵ model (Duynkerke 1988). In the entropy equation the heating or cooling due to the radiative flux divergence is included; a model is used for both longwave and shortwave radiation.

For longwave radiation we use the emissivity or "greybody" approximation to calculate the longwave radiative flux. The effect of water vapor, carbon dioxide, and liquid water on the emissivity is taken into account. The shortwave model includes Rayleigh scattering, absorption by atmospheric gases (water vapor, ozone, and CO_2), and absorption and scattering by cloud droplets. Further details on the radiation model are given in Duynkerke and Driedonks (1988).

3. Initialization

The model simulation was started at 1000 UTC 14 July 1987 just before the observations of Hignett (1991). The location of San Nicolas Island is 33.25°N, 119.5°W (Fig. 1). At the sea surface the roughness length is set to 2×10^{-4} m, and the albedo to 0.05. The sea surface temperature is taken as 288.4 K, which is obtained from extrapolating the observed sensible heat fluxes with the flux-profile relationships toward the surface. The specific humidity at the sea surface is set to its saturated value at the sea surface temperature.

In the one-dimensional model the subsidence has to be prescribed. Observations of the large-scale velocity field or vertical velocity field are lacking. Neiburger (1960) showed that climatologically the normal sea level pressure distribution over the eastern part of the North Pacific Ocean for July is anticyclonic with the pressure center at 38°N, 150°W. Moreover, the winds deviate far from the isobars over this area, giving an area of significant divergence off the California coast. While the divergence has a maximum along the California coast, it decreases in all directions over the ocean, but the divergence remains positive over practically all of the eastern part of the North Pacific Ocean. From Fig. 6 of Neiburger (1960) we get an average value for the divergence of 6×10^{-6} s^{-1} for July over San Nicolas Island.

From observations made during the Barbados Oceanographic and Meteorological Experiment (BOMEX), it is known that large diurnal variation in horizontal divergence can be present over large ocean areas that are relatively remote from major landmasses. Nitta and Esbensen (1974) found from rawinsonde observations for BOMEX phase 3 an amplitude in the horizontal divergence of about 3×10^{-6} s^{-1} at around 900 hPa, whereas the daily averaged subsidence was close to zero. Temporal variations in the divergence of this magnitude would have a tremendous influence on the stratocumulus field if it were present over the FIRE region, especially on cloud-top height. We have investigated whether such temporal variation is also present in the European Centre for Medium-Range Weather Forecasts (ECMWF) analysis for the two days under consideration.

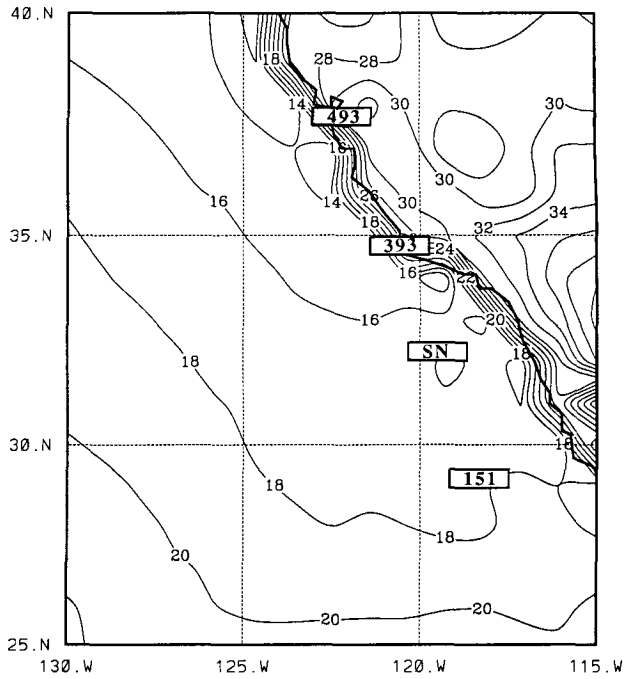

FIG. 1. Surface temperature analysis from the ECMWF model at 1800 UTC 14 July 1987. Indicated are the location of San Nicolas Island (SN) and the radiosonde stations Vandenberg AFB (393), Oakland metropolitan (493), and Isla Guadalupe (151).

We think that the best possible estimate for the vertical velocity field can be obtained from the analysis of the global ECMWF model. Although only a few radiosonde stations [i.e., Vandenberg AFB (393), Oakland metropolitan (493), and Isla Guadalupe (151), indicated in Fig. 1] are available over these large ocean areas, it is the best possible estimate we can obtain. Here, we will use the analysis of the vertical velocity at the model levels (at about the 0-, 66-, 227-, 540-,1042-, 1740-, 2650-, and 3770-m heights) at 1800 UTC 14 July 1987. In Fig. 2 we have shown the analysis of the vertical velocity at 33°N,120°W and 33°N,121°W, respectively. Figure 2 also shows the vertical velocity profile used in the model simulation, which is equivalent to a constant divergence with height of 3.5×10^{-6} s^{-1}.

The observed mean wind direction in the boundary layer is about 290° (Hignett 1991). In the upstream direction, the divergence from the ECMWF analysis is nearly constant over several hundreds of kilometers. So, if the simulation would be in a Lagrangian framework, in which the column of air is advected along

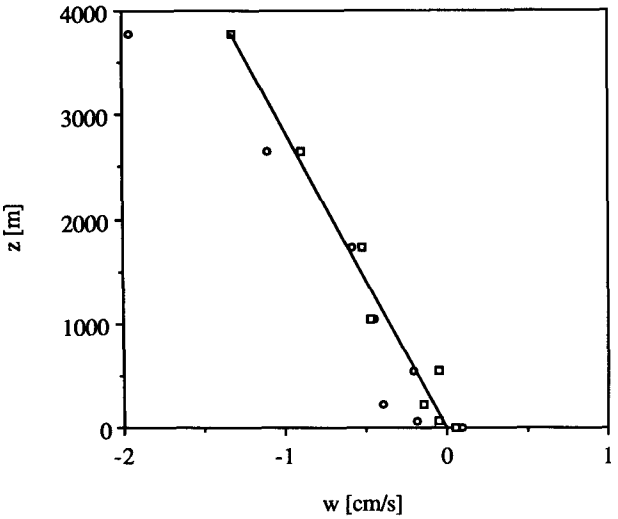

FIG. 2. Vertical velocity profile at 33°N, 120°W (squares) and 33°N, 121°W (circles) derived from the analysis of the ECMWF model at 1800 UTC 14 July 1987 and the profile used in the model simulation corresponding to a constant divergence of 3.5×10^{-6} s^{-1} with height.

with the mean wind, the divergence would be fairly constant along the trajectory.

The geostrophic wind speed was set to 5.5 m s^{-1} (Hignett 1991), and the wind direction to 290°. The wind is therefore blowing almost parallel to the isotherms of the sea surface temperature (Fig. 1). This means that the surface temperature hardly changes as the air flows southeastward. Therefore, it is quite realistic to keep the sea surface temperature in the one-dimensional model constant with time. The initial wet equivalent potential temperature and total specific humidity profile are taken to closely fit the observed profiles. We used the Cross-chain Loran Atmospheric Sounding System (CLASS) data up to 2 km of Schubert et al. (1987a). The vertical profiles of θ_q and q_w at 0014 and 1158 UTC 14 July and 0015, 1200, 1703, and 1935 UTC 15 July are shown in Fig. 3. We clearly see a well-mixed boundary layer with a strong capping inversion. The boundary layer is moist with a dry overlying atmosphere. The temperature jump at the inversion is about 12 K (Hignett 1991). For the initial model profiles we take $\theta_q = 314$ K within the boundary layer and $\theta_q = 323$ K above it. The specific humidity is taken as 9.6×10^{-3} kg kg^{-1} in the boundary layer, and just above, it is set to 7.6×10^{-3} kg kg^{-1}, with a lapse rate of -4×10^{-6} m^{-1} above the inversion. These initial θ_q and q_w profiles are shown as full thick lines in Fig. 3. The model top is taken as 1300 m.

4. Results and discussion

We will concentrate on the diurnal variation of the stratocumulus deck due to the decoupling of the cloud layer from the subcloud layer as observed during FIRE. More specifically, we will use the observations of 14 and 15 July 1987 and compare those with a model simulation. During this period, a steady northwesterly flow was observed at San Nicolas Island, which reduces the possibility of a coastal effect on the diurnal variation observed from the island.

In section 4a we will discuss the observed and simulated variation of cloud base, cloud top, liquid water path, and shortwave radiation at the surface. In section 4b we will discuss in more detail the cause of the diurnal variation, that is, the decoupling of the cloud layer from the subcloud layer. Moreover, the modeled and observed turbulent quantities will be compared. In section 4c we will discuss the influence of the decoupling on the surface fluxes, etc.

a. *Diurnal variation*

To study the time evolution of clouds during the FIRE experiment several instruments were used on San

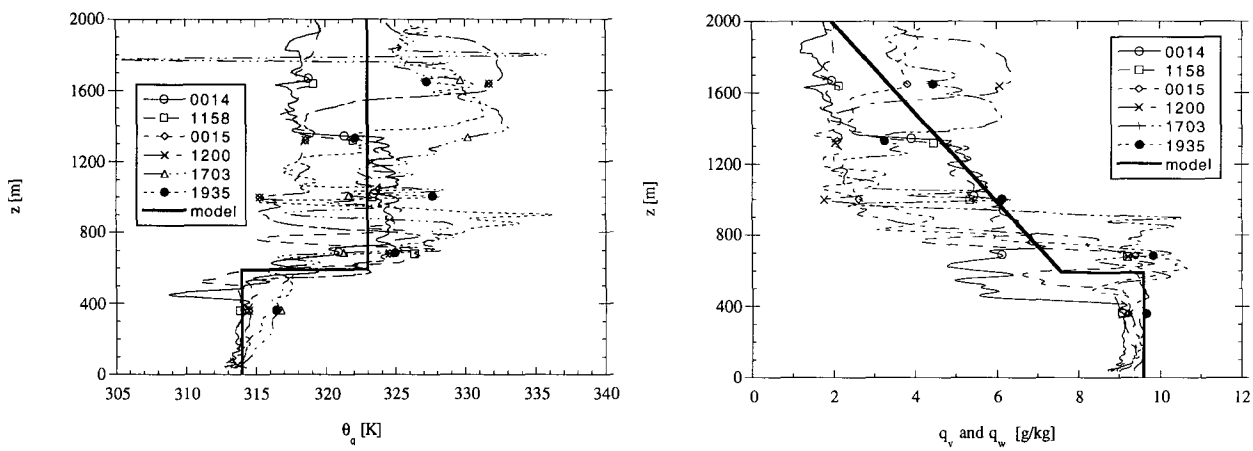

FIG. 3. The observed vertical profiles of (a) θ_q and (b) q_v at 0014 and 1158 UTC 14 July and 0015, 1200, 1703, and 1935 UTC 15 July and the initial profiles of θ_q and q_w used in the model simulation (full thick lines).

Nicolas Island to monitor cloud properties with a high temporal resolution. Cloud-base height was measured by a Vaisala CT 12K laser ceilometer operated by Colorado State University as described by Schubert et al. (1987b). The ceilometer operated continuously and gave cloud base height every 30 s.

A sodar was used to estimate the inversion height (White 1989). The height was determined where the maximum in the reflectivity of an acoustic signal occurred. This is at the height of the temperature inversion, which is then associated with the height of cloud top.

The vertically integrated liquid water content was retrieved using a three-channel (20.6, 21.65, and 90.0 GHz) microwave radiometer as described by Hogg et al. (1983). A statistical algorithm converts recorded brightness temperature of the atmosphere into path-integrated liquid water (liquid water path). The absolute uncertainty in the instrument is estimated to be 20%. The radiometer yielded nearly continuous measurements throughout the FIRE period with a time resolution of 1 min.

The variation of cloud base and top height, as retrieved from the ceilometer and the sodar, is shown in Fig. 4a as a function of time for 13, 14, 15, and 16 July 1987. To indicate time continuously in the figures, we have denoted the period from 0000 UTC 13 July to 2400 UTC 16 July as −2400 to 7200. We have used 0000 for 0000 UTC 14 July because we start our simulation on 14 July. As can be seen from Fig. 4a, the cloud thickness increases during the period under consideration. Moreover, there are variations in cloud thickness on the time scale of a day or less. We are mainly interested in the latter variations and not in the slow variations on the time scale of a day or more, which are probably due to changes in the synoptic circulation (subsidence) in the area under consideration. To highlight the diurnal variability of the cloud rather than the slow changes due to the synoptic observations, we have objectively removed the effect of the long-term trend. We have detrended cloud-top and cloud-base height by calculating for each hourly value the departure from the 24-h mean around that value. These departures were then added to the overall mean of the 4-day period, producing the results shown in Fig. 4b. The observed average cloud-top height is 585 m, and the average cloud-base height is 238 m.

The simulated cloud-base height (Fig. 4b) shows more or less the same variations as the observations with time. Noon is around 2000 UTC, with sunrise and sunset occurring at about 1300 and 2700, respectively. It is clear that in both the observations and model results the cloud-base lifting sets in some hours after sunrise. The maximum cloud-base lifting takes place in the late afternoon. After this, the cloud-base descent sets in, lasting until midnight. It is clear that the diurnal changes do not follow the solar insolation directly, in the sense that they are not symmetrically around local solar noon. This is not surprising since the largest solar heating rates and therefore the largest changes in cloud base height are expected around solar noon. This can be seen in both the observations and simulation results shown in Fig. 4b.

For the optical properties of the cloud, the liquid water path (the vertically integrated liquid water content) is an important quantity to consider (Stephens 1984). Typically, the liquid water content varies linearly with height with the vertical gradient equal to $(\partial q_{\text{sat}}/\partial T)_T \partial T/\partial z$. This gives that the liquid water path is proportional to the cloud layer thickness squared (Blaskovic et al. 1991). The liquid water path will therefore show a much larger temporal variation than the cloud thickness. The observed and simulated liquid water path is shown in Fig. 5 as a function of time. The simulated liquid water path typically varies between 0.2 mm at around sunrise to about 0.02 mm

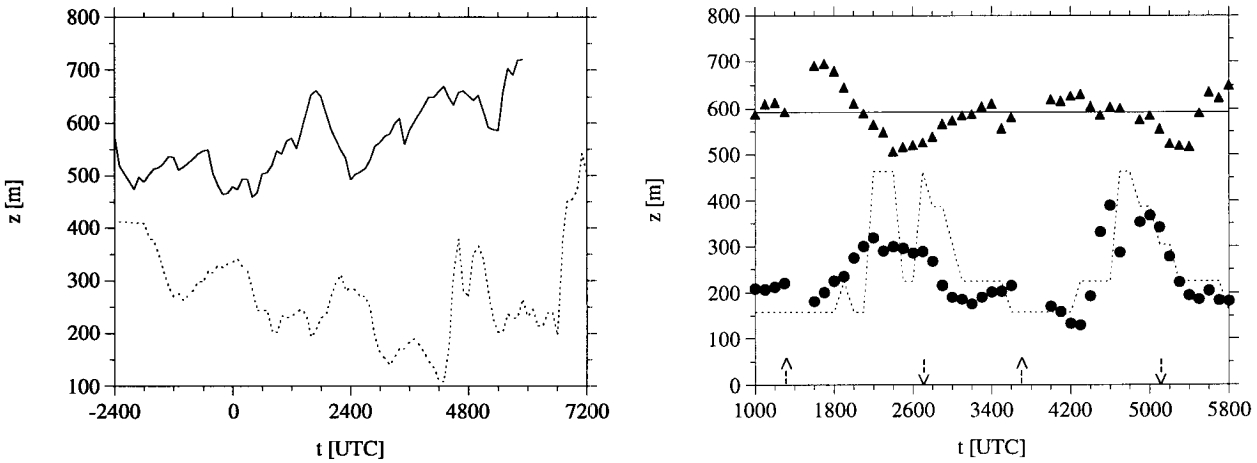

FIG. 4. (a) Time evolution of the observed cloud top and base height. (b) The detrended observed (symbols) and simulated (lines) cloud top and base height as a function of time. Sunrise and sunset are indicated by an upward and downward arrow, respectively.

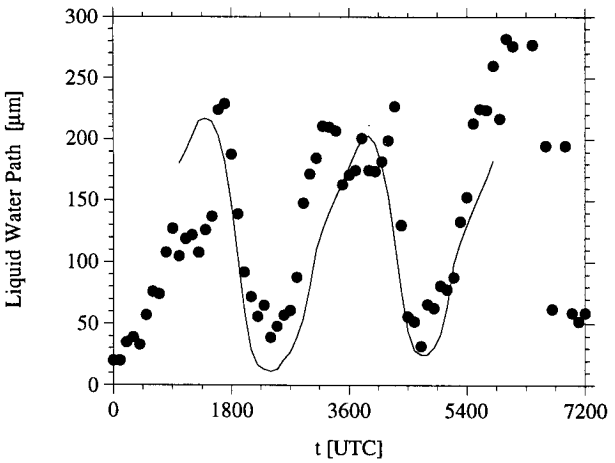

FIG. 5. The observed (dots) hourly averaged liquid water path compared with the model-simulated (full line) liquid water path as a function of time.

some hours before sunset. The observations show a similar kind of diurnal variation. In the model simulation the liquid water path is typically very close to the adiabatic liquid water path, very similar to that in the observations (Albrecht et al. 1990). The largest difference between the simulated liquid water path and the adiabatic value occurs from 1500 to 2400 UTC, which is during the decoupling of the cloud layer from the subcloud layer.

As a result of the large diurnal variation in cloud thickness and liquid water content also, the downward shortwave radiation does not vary symmetrically around solar noon (Fig. 6). In the model simulation the maximum solar insolation at the surface is reached at about 2200 UTC, two hours after local noon.

b. Turbulent structure and vertical profiles

In the previous section we compared the simulated with the observed temporal evolution of cloud-top height, cloud-base height, liquid water path, and downwelling shortwave radiation at the surface. In this section we will discuss in somewhat more detail what causes the diurnal variation. We will do this by looking at the simulated vertical structure of the boundary layer. Moreover, we make some comparisons with the observations of Hignett (1991).

Hignett (1991) presented measurements made during FIRE by instruments attached to the cable of a tethered balloon. The data were selected for a day and a night period, corresponding to 1830–2100 UTC (14 July) for the daytime and 0530–0800 UTC (15 July) for the night. Local noon occurred at about 2000 UTC. He showed that during daytime the boundary layer was decoupled into a separate cloudy layer and a surface (subcloud) layer.

The periods chosen for comparison by Hignett (1991) were centered around local noon and midnight. These times are the extremes of the external forcing from solar radiation but do not correspond to the extremes of the resulting diurnal cycle of cloud thickness and liquid water path. However, these periods do represent decoupled and coupled cases and have been chosen for a direct comparison between the observations and simulation.

Hignett (1991) used the vertical velocity variance as an indicator of convective activity. Since in the model only the turbulent kinetic energy is calculated and we have no means to separate this into the variances in the different directions, we have plotted both the simulated and observed (both at 3200 and 4500 UTC) turbulent kinetic energy in Fig. 7a, whereas, the observed vertical velocity variance at these times is plotted in Fig. 7b. It can be clearly seen that during the night the boundary layer is turbulent up to cloud top, whereas during daytime the turbulent kinetic energy decreases from the surface upward to near zero below cloud base. The cloud layer is turbulent due to the convection initiated by the longwave radiative cooling at cloud top. The nocturnal boundary layer is thus a well-mixed layer from the inversion to the surface, driven from cloud top (by longwave radiative cooling) in a manner analogous to that of a convective boundary layer heated from below.

All these features are also reflected in the turbulent fluxes of conserved quantities (q_w, θ_q), total water content, and wet equivalent potential temperature (Pointin 1984), respectively. As an example, we have shown in Fig. 8a the simulated and observed vertical profiles of the wet equivalent potential temperature flux. The simulated fluxes at the surface are positive. The flux maxima are located at cloud top, with the larger fluxes occurring during the night. The nocturnal data again give the appearance of a single well-mixed layer driven by the longwave radiative cooling at cloud top. The

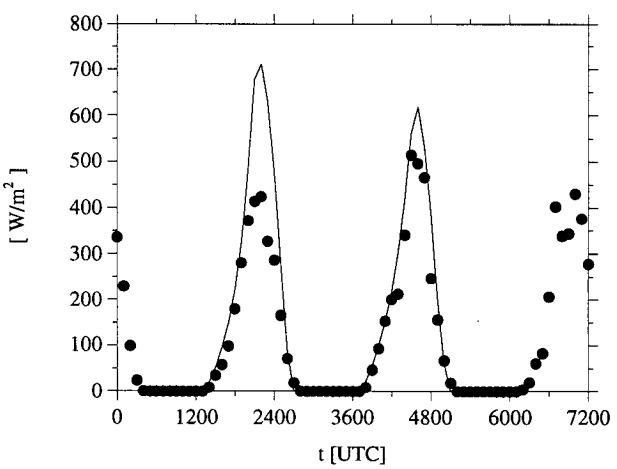

FIG. 6. The measured (dots) downwelling shortwave radiation at the surface compared with the simulated (line) shortwave radiation as a function of time.

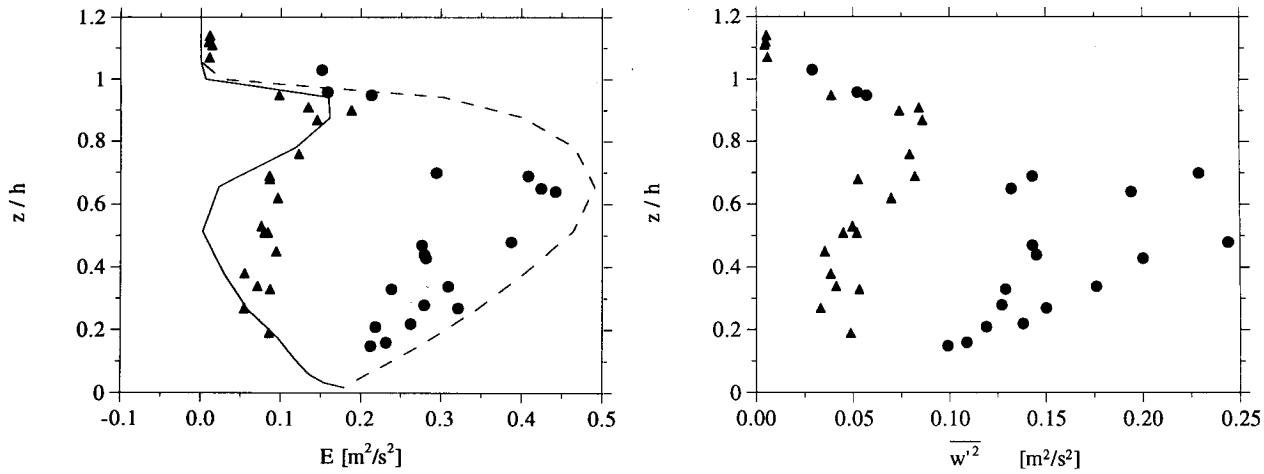

FIG. 7. (a) The simulated (lines) and observed (symbols) turbulent kinetic energy at 3200 (dashed line and dots) and 4500 UTC (full line and triangles) as a function of dimensionless height. (b) The observed vertical velocity variance at 3200 (dots) and 4500 UTC (triangles) as a function of dimensionless height.

daytime profile shows clearly two turbulent layers: a surface layer and a cloud layer. This structure is also observed in the simulated total moisture flux that is shown in Fig. 8b. The cloud layer is driven by the cloud-top cooling, whereas the surface layer is mainly driven by shear.

The turbulent structure of the stratocumulus-topped atmospheric boundary layer can be studied in more detail through the inspection of the turbulent kinetic energy budget. In one-dimensional form the equation for the turbulent kinetic energy (Duynkerke and Driedonks 1988) reads

$$\frac{\partial E}{\partial t} = \underbrace{-\overline{u'w'}\frac{\partial u}{\partial z} - \overline{v'w'}\frac{\partial v}{\partial z}}_{\text{S}} \underbrace{- g\frac{\overline{w'\rho'}}{\rho_0}}_{\text{B}} - w\frac{\partial E}{\partial z} \underbrace{- \frac{\partial}{\partial z}\left(\overline{w'E'} + \frac{\overline{w'p'}}{\rho_0}\right)}_{\text{T}} \underbrace{- \epsilon}_{\text{D}}, \quad (4.1)$$

in which the terms on the right-hand side are the shear production (S), buoyancy production (B), vertical advection (subsidence), turbulent transport (T), and viscous dissipation (D).

In Figs. 9a,b the simulated and observed terms in the turbulent kinetic energy budget are compared. For the observations the terms in (4.1) were evaluated as described by Nicholls (1985). During the night (3200 UTC, Fig. 9a), the turbulence is mainly driven by the longwave radiative cooling at cloud top. This gives convection throughout the whole boundary layer as can be seen from the positive values of the buoyancy production from cloud top down to the sea surface. Close to the surface the buoyancy production is small because there is only a small difference between the sea surface and the air just above it. In the model the transport term is negative (sink) in the cloud layer and positive at the inversion and in the subcloud layer. The observations show a somewhat opposite trend. However, this might be due to the fact that it includes only the divergence of $\overline{w'E'}$ and not the term $\overline{w'p'}/\rho_0$. The latter term cannot be evaluated from the observations, because the pressure fluctuations are not measured. The modeled and observed transport terms (T) do not represent the same quantities. The observed viscous dissipation in the subcloud layer is larger than the simulated viscous dissipation. As a result, it is clear that in the observations there is a large imbalance between the sum of all the terms; overall, the picture appears similar to that described by Nicholls (1989).

During daytime (4500 UTC, Fig. 9b), the longwave radiative cooling is about the same as during nighttime because the cloud is still optically thick for longwave radiation (Fig. 10). The main difference is the shortwave radiative heating of the cloud layer. This heating is mainly distributed over a layer with a thickness of about 200 m near cloud top. As a result, the shortwave radiative heating offsets part of the longwave radiative cooling in the upper 50 m of the cloud layer. Below this the shortwave radiative heating is dominant. If the boundary layer remains well mixed, this means that the buoyancy production near cloud base will diminish, and if the divergence in the shortwave radiation is large enough, it can make the buoyancy flux near cloud base negative. This implies that the convection is suppressed and as a result the turbulent transport of momentum, heat, and moisture will be reduced. Both the observations and simulations (Fig. 9b) show that the buoyancy production is mainly localized inside the cloud layer, where it is balanced by turbulent transport and

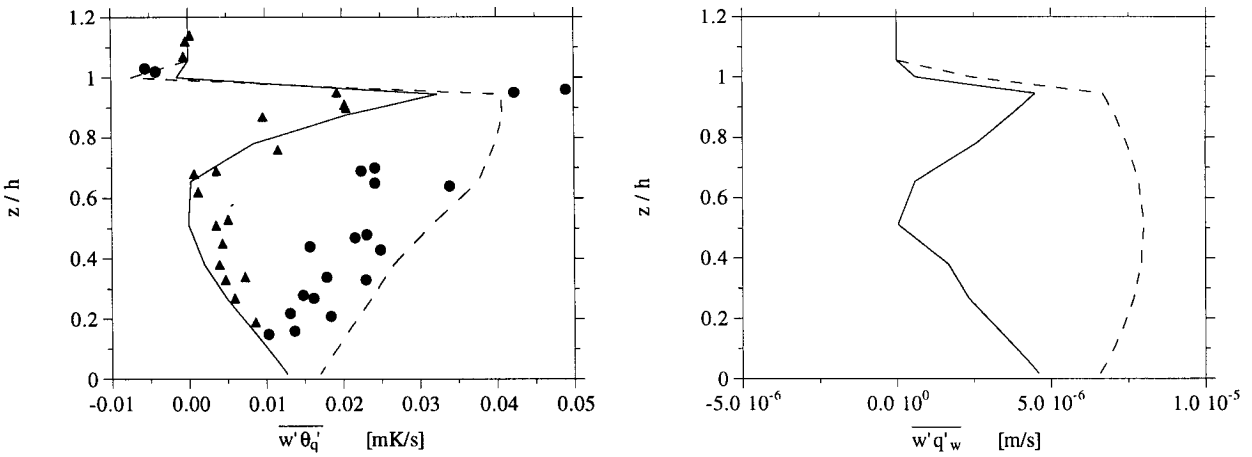

FIG. 8. (a) The simulated (lines) and observed (symbols) equivalent potential temperature flux at 3200 (dashed line and dots) and 4500 UTC (full line and triangles) as a function of dimensionless height. (b) The simulated (lines) total moisture flux at 3200 (dashed line) and 4500 UTC (full line) as a function of dimensionless height.

viscous dissipation. The simulated turbulent kinetic energy budget clearly shows a three-layer structure in the boundary layer: a turbulent layer connected to the surface mainly driven by shear, a convective cloud layer mainly driven by longwave radiative cooling at cloud top, and in between a transition layer that is near neutral to slightly stable, where all the production terms are very small. For this daytime case the simulated results are in rather good agreement with the observations. Moreover, the observed terms in the turbulent kinetic energy budget are in quite close balance, which gives good confidence in the quality of the data.

c. *Consequences of diurnal variation*

Both observations and detailed models are expected to provide guidelines for developing simpler models. Standard mixed-layer models are clearly inadequate to describe the decoupling of the cloud layer and the subcloud layer. Turton and Nicholls (1987) developed a model in which the single mixed layer observed during nighttime was diagnosed to split into two mixed layers during daytime. The criterion used to diagnose this decoupling is that the maximum allowable energy loss against negative buoyancy is a fraction (40%) of the buoyancy produced in the cloud layer. In this way the height of the base of the mixed layer produced by the cloud convection can be calculated. Turton and Nicholls (1987) showed that the introduction of these two separately well mixed, but decoupled, layers produced a significant diurnal variation in cloud thickness. When separation is not allowed, the cloud thickness varies only slowly and the diurnal variation is mainly due to the variation in entrainment velocity.

In cloud-free mixed layers the entrainment velocity w_e is found to depend mainly on the properties of the turbulence-maintaining entrainment and the density difference across the interface ($\Delta\rho$). Many investigations have been carried out with turbulence being driven by a variety of processes: mechanical stirring with grids, surface shear stress, convection resulting from surface heating, and shear across the interface. Dimensional arguments (Turner 1973) suggest that in these experiments involving a dominant turbulence production mechanism with a length scale l and velocity scale U, the entrainment velocity scales as (Nelson et al. 1989; Wilde et al. 1985)

$$\frac{w_e}{U} = f(\mathrm{Ri}_U) = f\left(-\frac{g}{\rho_0}\frac{\Delta\rho l}{U^2}\right), \tag{4.2}$$

in which Ri_U is the Richardson number.

In geophysical applications l is usually taken as the mixed-layer depth h, and for the velocity scale, u^* is used for shear-driven layers and w^* for a convectively driven layer. For the convectively driven case, which we will consider, the most widely used result is

$$\frac{w_e}{w^*} = \frac{a}{\mathrm{Ri}_{w^*}}, \tag{4.3}$$

with $\mathrm{Ri}_{w^*} = (g/\theta_v)(\Delta\theta_v h/w_*^2)$, with values of $a = 0.2$–0.25 (Driedonks 1982; Deardorff 1983) for the cloud-free case and model-derived values of about 2 for the cloudy case (Nicholls and Turton 1986). The hourly values from the model simulation are shown in Fig. 11 and indicate a value of about 0.15 for a in (4.3). These values seem rather low compared with the values of Nicholls and Turton (1986). The variation of w_e as a function of time is shown in Fig. 12. The entrainment velocity is thus very small during daytime and has a value of about 0.2 cm s^{-1} during nighttime. These simulated entrainment velocities are of the same magnitude as those observed by Kawa and Pearson (1989) during the DYCOMS (dynamics and

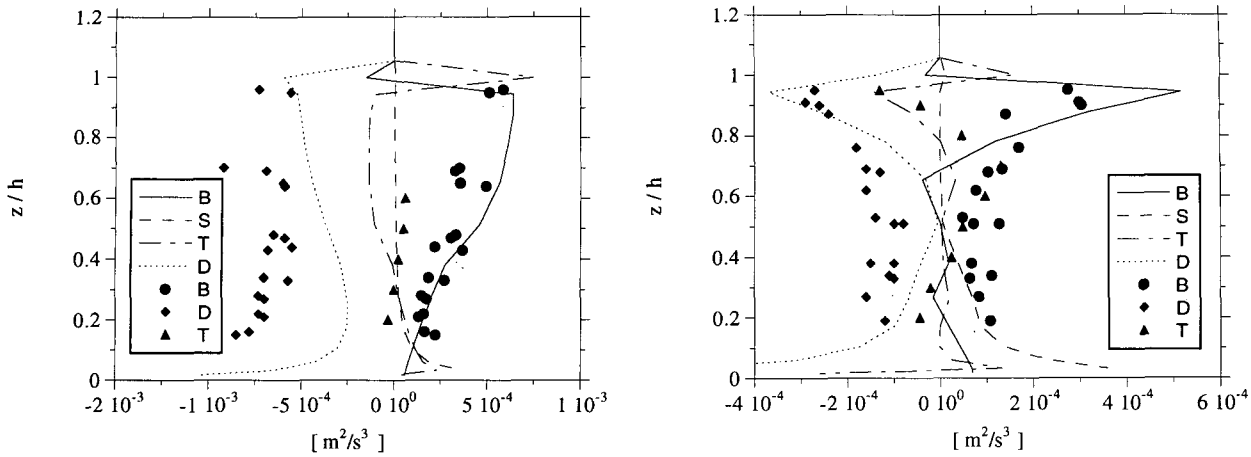

FIG. 9. The simulated (lines) and observed (symbols) turbulent kinetic energy budget as a function of height (normalized by the inversion depth) for the (a) nighttime and (b) daytime period: buoyancy production (B), shear production (S), turbulent transport (T), and viscous dissipation (D).

chemistry of marine stratocumulus) experiment. These observations are taken in the same region (from 30° to 35°N and from 120° to 125°W) as the FIRE observations. Ten flights were made off the southern California coast in July and August 1985, most of which took place around solar noon. From measured ozone fluxes and the "jump" in ozone concentration across the inversion, Kawa and Pearson (1989) calculated the entrainment rates (their Table 1). The observed entrainment rates vary from 0 to 0.5 cm s^{-1}, with an average value of 0.3 cm s^{-1}. During DYCOMS the inversion strength was about 5 K, whereas during the observational period of FIRE considered in this paper the inversion strength was about 12 K. Given that the convective velocity w^*, which is mainly determined by the longwave radiative cooling at cloud top, is about the same, this would mean that the entrainment velocity during FIRE was 2.4 times smaller than during DYCOMS. This is in good agreement with the values shown in Fig. 12.

The diurnal variation in cloud and turbulence properties also gives a diurnal variation in the surface fluxes as shown in Fig. 13. The sensible (H) and latent (LE) heat flux show a maximum around sunrise and a minimum around sunset. This is mainly a result of the decoupling of the cloud layer from the subcloud layer. During nighttime the convection through the whole boundary layer is driven by the cloud-top radiative cooling. This longwave cooling cools the boundary layer and as a result the temperature difference between the sea surface and the air just above it will increase

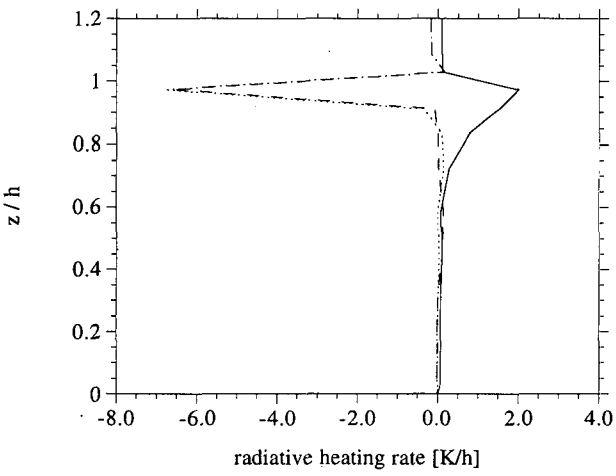

FIG. 10. The shortwave radiative heating profile at 4500 UTC (full line) and the longwave radiative cooling profile at 3200 UTC (long dashed) and 4500 UTC (short dashed) as a function of dimensionless height.

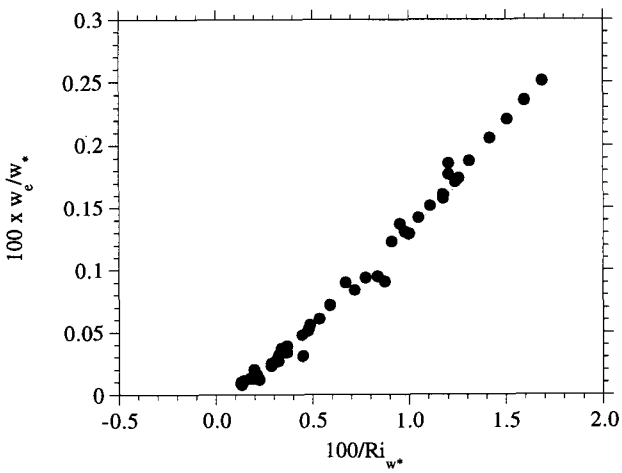

FIG. 11. The simulated dimensionless entrainment velocity as a function of the inverse of the Richardson number given by Eq. (4.3).

giving rise to an increasing sensible heat flux with time. During daytime the cloud layer and the turbulent layer adjacent to the sea surface become decoupled, so that the longwave cooling can no longer cool the turbulent layer adjacent to the sea surface. Moreover, the dominant process that can change the temperature of this layer is the sensible heat flux from the sea surface. As a result, the temperature of this layer increases and the temperature difference with the sea surface diminishes, with the result that the sensible heat flux decreases toward zero.

5. Conclusions

A comparison between the results of a model simulation and detailed measurements of the diurnal cycle of a marine stratocumulus-capped boundary layer during the 1987 FIRE have been made. In the model simulation the decoupling is caused by the absorption of solar radiation in the cloud layer. The decoupling of the boundary layer into a separate cloud and subcloud layer is most pronounced from noon to just before sunset. The decoupling is very similar to the previously reported observations of Nicholls (1984) and Nicholls and Leighton (1986).

During both daytime and nighttime, the simulated and observed turbulent kinetic energy budgets are compared. The multiple-level turbulence measurements, made simultaneously from a series of probes attached to the cable of a tethered balloon, give a detailed vertical profile of the most important terms in the turbulent kinetic energy budget. Both the observations and the simulation reveal that during nighttime the boundary layer is well mixed. With a small surface buoyancy flux, the turbulence is mainly driven by the longwave radiative cooling at cloud top, giving buoyancy production throughout the boundary layer.

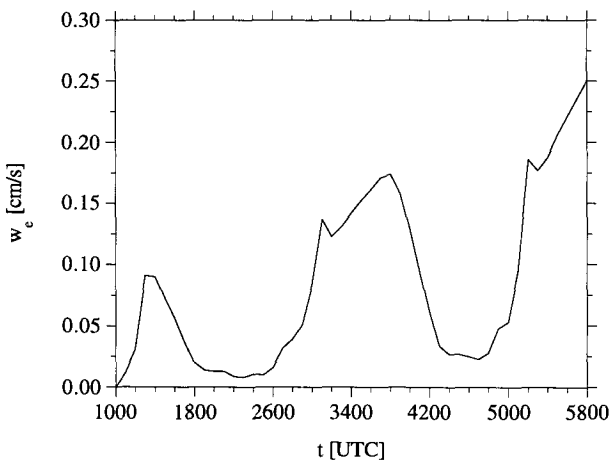

FIG. 12. The entrainment velocity w_e (cm s^{-1}) as a function of time.

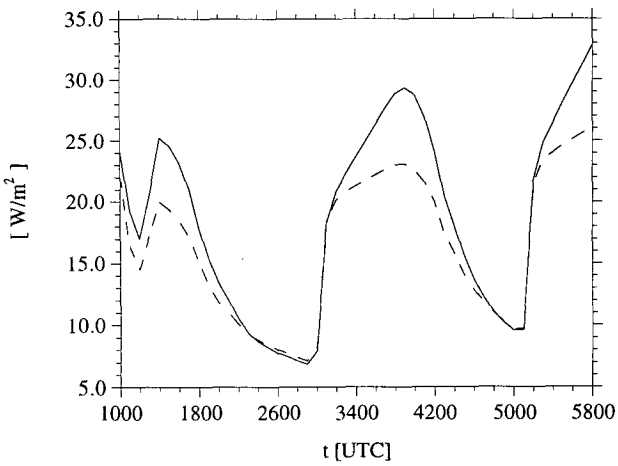

FIG. 13. The latent heat flux LE (dashed line) and the sum of sensible and latent heat flux H + LE (full line) as a function of time.

During daytime the absorption of solar radiation in the cloud layer gives rise to the formation of a stable layer below cloud base. Both the observations and the simulation show that the buoyancy production is mainly localized in the cloud layer. The simulated turbulent kinetic energy budget clearly shows a three-layer structure in the boundary layer: a turbulent surface mixed layer driven by wind shear, a convective cloud layer, and, in between, a transition layer. In this transition layer all production terms are very small and the stratification is from near neutral to slightly stable.

Acknowledgments. Most of this work was done when P. G. Duynkerke worked as a visiting scientist in the group of Graeme Stephens (Department of Atmospheric Sciences, Colorado State University) during the summer of 1991. This visit was made possible due to the financial assistance of Graeme Stephens (ONR N00014-91-J-1422) and the Netherlands Organization for Scientific Research. P. G. Duynkerke thanks Susan Lini for organizing his stay and all the arrangements she made during the visit. Moreover, we want to thank Bruce Albrecht and Wayne Schubert for supplying us with the observational data obtained during FIRE.

REFERENCES

Albrecht, B. A., C. W. Fairall, D. W. Thomson, A. B. White, J. B. Snider, and W. H. Schubert, 1990: Surface-based remote sensing of the observed and the adiabatic liquid water content of stratocumulus clouds. *Geophys. Res. Lett.*, **17**, 89–92.

Betts, A. K., 1989: The diurnal variation of California coastal stratocumulus for two days of boundary layer soundings. *Tellus*, **42A**, 302–304.

Blaskovic, M., R. Davies, and J. B. Snider, 1991: Diurnal variation of marine stratocumulus over San Nicolas Island during July 1987. *Mon. Wea. Rev.*, **119**, 1469–1478.

Bougeault, P., 1985: The diurnal cycle of the marine stratocumulus layer: A higher-order model study. *J. Atmos. Sci.*, **42**, 2826–2843.

Deardorff, J. W., 1983: A multi-limit mixed layer entrainment formulation. *J. Phys. Oceanogr.*, **13,** 988–1002.

Driedonks, A. G. M., 1982: Models and observations of the growth of the atmospheric boundary layer. *Bound.-Layer Meteor.*, **23,** 283–306.

Duynkerke, P. G., 1988: Application of the E–ϵ turbulence closure model to the neutral and stable atmospheric boundary layer. *J. Atmos. Sci.*, **45,** 865–880.

——, 1990: The diurnal variation of a stratocumulus layer: A model sensitivity study. *Mon. Wea. Rev.*, **117,** 1710–1725.

——, and A. G. M. Driedonks, 1987: A model for the turbulent structure of the stratocumulus-topped atmospheric boundary layer. *J. Atmos. Sci.*, **44,** 44–62.

——, and ——, 1988: Turbulent structure of a shear driven stratus-topped atmospheric boundary layer: A comparison of model results with observations. *J. Atmos. Sci.*, **45,** 2343–2351.

Hignett, P., 1991: Observations of the diurnal variation in a cloud-capped marine boundary layer. *J. Atmos. Sci.*, **48,** 1474–1482.

Hogg, D. C., F. O. Guiraud, J. B. Snider, M. T. Decker, and E. R. Westwater, 1983: A steerable dual-channel microwave radiometer for measurements of water vapor and liquid in the troposphere. *J. Climate Appl. Meteor.*, **22,** 789–806.

Kawa, S. R., and R. Pearson, Jr., 1989: An observational study of stratocumulus entrainment and thermodynamics. *J. Atmos. Sci.*, **46,** 2649–2661.

Neiburger, M., 1960: The relation of air mass structure to the field of motion over the eastern North Pacific Ocean in summer. *Tellus,* **12,** 31–40.

Nelson, E., R. B. Stull, and E. Eloranta, 1989: A prognostic relationship for entrainment zone thickness. *J. Appl. Meteor.*, **28,** 885–903.

Nicholls, S., 1984: The dynamics of stratocumulus: Aircraft observations and comparison with a mixed-layer model. *Quart. J. Roy. Meteor. Soc.*, **110,** 783–820.

——, 1985: Aircraft observations of the Ekman layer during the Joint Air–Sea Interaction Experiment. *Quart. J. Roy. Meteor. Soc.*, **111,** 391–426.

——, 1989: The structure of radiatively driven convection in stratocumulus. *Quart. J. Roy. Meteor. Soc.*, **115,** 487–511.

——, and J. Leighton, 1986: An observational study of stratiform cloud sheets. Part I: Structure. *Quart. J. Roy. Meteor. Soc.*, **112,** 431–460.

——, and J. D. Turton, 1986: An observational study of the structure of stratiform cloud sheets. Part II: Entrainment. *Quart. J. Roy. Meteor. Soc.*, **112,** 461–480.

Nitta, T., and S. Esbensen, 1974: Diurnal variation in the western atlantic trades during the BOMEX. *J. Meteor. Soc. Japan,* **52,** 254–257.

Pointin, Y., 1984: Wet equivalent potential temperature and enthalpy as prognostic variables in cloud modeling. *J. Atmos. Sci.*, **41,** 651–660.

Randall, D. A., Harshvardhan, and D. A. Dazlich, 1991: Diurnal variability of the hydrologic cycle in a general circulation model. *J. Atmos. Sci.*, **48,** 40–62.

Schubert, W. H., P. E. Ciesielski, T. B. McKee, J. D. Kleist, S. K. Cox, C. M. Johnson-Pasqua, and W. L. Smith, Jr., 1987a: Analysis of boundary layer sounding data from the FIRE marine stratocumulus project. Colorado State University, Atmospheric Science Paper No. 419, 101 pp.

——, S. K. Cox, P. E. Ciesielski, and C. M. Johnson-Pasqua, 1987b: Operation of a ceilometer during the FIRE marine stratocumulus experiment. Colorado State University, Atmospheric Science Paper No. 420, 34 pp.

Stephens, G. L., 1984: The parameterization of radiation for numerical weather prediction and climate models. *Mon. Wea. Rev.*, **112,** 826–867.

Turner, J. S., 1973: *Buoyancy Effects in Fluids.* Cambridge University Press, 368 pp.

Turton, J. D., and S. Nicholls, 1987: A study of the diurnal variation of stratocumulus using a mixed layer model. *Quart. J. Roy. Meteor. Soc.*, **113,** 969–1009.

White, A. B., 1989: Temperature and humidity structure parameters deduced from sodar and radar reflectivities: An analysis of data from the marine stratocumulus phase of FIRE. M.S. thesis, Department of Meteorology, Pennsylvania State University, 137 pp.

Wilde, N. P., R. B. Stull, and E. W. Eloranta, 1985: The LCL zone and cumulus onset. *J. Climate Appl. Meteor.*, **24,** 640–657.